JOM, Vol. 69, No. 12, 2017
DOI: 10.1007/s11837-017-2599-9

New Development in Selective Laser Melting of Ti–6Al–4V: A Wider Processing Window for the Achievement of Fully Lamellar $\alpha + \beta$ Microstructures

E.W. LUI,[1] W. XU,[1,2,3] A. PATERAS,[1] M. QIAN,[1,4] and M. BRANDT[1]

1.—Centre for Additive Manufacturing, School of Engineering, RMIT University, Melbourne, VIC 3000, Australia. 2.—School of Engineering, Macquarie University, Sydney, NSW 2109, Australia. 3.—e-mail: wei.xu@mq.edu.au. 4.—e-mail: ma.qian@rmit.edu.au

Recent progress has shown that Ti–6Al–4V fabricated by selective laser melting (SLM) can achieve a fully lamellar $\alpha + \beta$ microstructure using 60 μm layer thickness in the as-built state via in situ martensite decomposition by manipulating the processing parameters. The potential to broaden the processing window was explored in this study by increasing the layer thickness to the less commonly used 90 μm. Fully lamellar $\alpha + \beta$ microstructures were produced in the as-built state using inter-layer times in the range of 1–12 s. Microstructural features such as the α-lath thickness and morphology were sensitive to both build height and inter-layer time. The α-laths produced using the inter-layer time of 1 s were much coarser than those produced with the inter-layer time of 12 s. The fine fully lamellar $\alpha + \beta$ structure resulted in tensile ductility of 11% and yield strength of 980 MPa. The tensile properties can be further improved by minimizing the presence of process-induced defects.

INTRODUCTION

Selective laser melting (SLM) is an established commercial powder-bed fusion additive manufacturing (AM) technique.[1] While a wide range of metals has been processed using AM, Ti–6Al–4V has gained the most attention because of its significant industrial applications and relatively high conventional manufacturing cost.[2] The mechanical performance of extra-low-interstitial (ELI) Ti–6Al–4V (< 0.13% O) is primarily determined by microstructural features such as their constituent phases, morphology and characteristic length scales. In the SLM of Ti–6Al–4V, the intrinsically rapid cooling rate of the melt pool usually results in a fully acicular α'-martensitic structure contained within columnar prior-β grains.[1,3] The α'-plates contain twins and dislocations and are supersaturated with V. Therefore, they often lead to both low tensile ductility (< 10%)[4] and low fracture toughness.[5] Thus, post-heat treatment is necessary to decompose martensite into an $\alpha + \beta$ microstructure for improved ductility[6] and toughness.[5]

Recent developments have shown that SLM Ti–6Al–4V in the as-built state can achieve a fully lamellar $\alpha + \beta$ microstructure via in situ martensite decomposition by manipulating SLM variables, including the focal off-set distance, energy density, inter-layer time and hatch spacing (the layer thickness was fixed at 60 μm).[7–10] In addition, tunable microstructural length scales and superior mechanical properties were achieved in SLM Ti–6Al–4V in the as-built state. These developments have made SLM of Ti–6Al–4V essentially similar to selective electron beam melting (SEBM) in terms of both the as-built microstructures and tensile properties.[8] This study builds on these recent findings and focuses on SLM of Ti–6Al–4V at the 90 μm layer thickness, which is less commonly used in SLM but offers potential advantages, e.g., allowing a wider processing window as well as use of coarser powder for improved cost-effectiveness.[11,12] For a fixed layer thickness, preliminary research has shown that the inter-layer time is most influential in determining in situ martensite decomposition during SLM of Ti–6Al–4V.[8] Consequently, this study focuses on

(Published online September 22, 2017)

investigating the effect of inter-layer time and build height on the microstructure and mechanical properties of SLM-fabricated Ti–6Al–4V.

EXPERIMENTAL

Spherical gas atomized ELI Ti–6Al–4V powder (25–45 μm, 0.1% O, 0.009% N, 0.008% C, 0.17% Fe, < 0.002% H, TLS Technik GmbH & Co.) was used to produce samples on a SLM 250 HL (SLM Solutions GmbH, argon flow, oxygen level < 0.1%, chamber temperature 200°C). For microstructural studies, a series of cylindrical rods (12 mm in diameter, 30 mm in height) with varying inter-layer times (t_i: 1, 8, 10 s) were vertically built onto fine lattice support structures (0.4 contact area ratio) at the laser power of 375 W, layer thickness of 90 μm, scanning velocity of 686 mm/s, focal offset of 2 mm, hatch spacing of 0.12 mm and energy density of 50.62 J/mm^3. Additionally, cylindrical rods of Ti–6Al–4V (12 mm in diameter, 75 mm in height, t_i: 1, 5, 12 s) were fabricated using the same parameters and machined into tensile specimens (gauge section dimensions: Ø 6 mm × 30 mm as per ASTM standard E8/E8 M-09). Uniaxial tensile testing was carried out with an initial strain rate of 2.5×10^{-4} s^{-1} on three specimens per build condition using a MTS universal testing machine (100 kN) attached with a laser extensometer. Characterization of microstructure and fracture surfaces was performed using an ultra-high-resolution scanning electron microscopy (SEM, FEI Verios 460L). Samples for SEM analysis (backscatter) were prepared by conventional grinding and polishing (without chemical etching). For the 30-mm-tall cylinders, specimens for microstructural analysis were obtained from the height of 15 mm, while, for the 75-mm-tall cylinders, they were extracted from two heights, 15 mm and 60 mm.

RESULTS AND DISCUSSION

Representative as-built microstructures of the 30-mm-tall sample are shown in Fig. 1. All samples achieved a fully $\alpha + \beta$ lamellar microstructure because of in situ martensite decomposition. The width of the α-laths depends strongly on the inter-layer time t_i, where increasing t_i often results in the formation of finer α-laths. For the 30-mm-tall samples, the use of t_i = 1 s (the shortest) led to the formation of coarser α-laths with an average thickness of 0.79 ± 0.26 μm (Fig. 2a). Increasing t_i from 1 s to 8 s resulted in finer α-laths of 0.52 ± 0.17 μm, while further prolonging t_i to 10 s led to a slight microstructural change with an average α-lath thickness of 0.54 ± 0.18 μm. This indicates that the variation in microstructure is minimal for t_i longer than 8 s in the 30-mm-tall sample made using a layer thickness of 90 μm.

The α-lath thickness at the build height of 15 mm in the 75-mm-tall samples followed a similar trend with increasing t_i (Fig. 2a). However, using t_i = 1 s resulted in much coarser α-laths (2.94 ± 0.97 μm, Figs. 2a and 3a) than those achieved at the height of 15 mm in the 30-mm-tall samples (0.79 ± 0.26 μm, Figs. 1a and 2a). The decrease in α-lath thickness with increasing t_i was also found to be more pronounced, being reduced by 71% with increasing t_i from 1 s to 5 s (0.84 ± 0.30 μm), followed by a further reduction of 65% from 5 s to 12 s (0.30 ± 0.09 μm). This indicates that in situ martensite decomposition during SLM of Ti–6Al–4V at the layer thickness of 90 μm is more sensitive to t_i for taller samples. The $\alpha + \beta$ lamellar microstructures produced in the 75-mm-tall samples were coarser than those in the 30-mm-tall samples (Figs. 3a versus 1a). To determine the microstructure homogeneity along the build

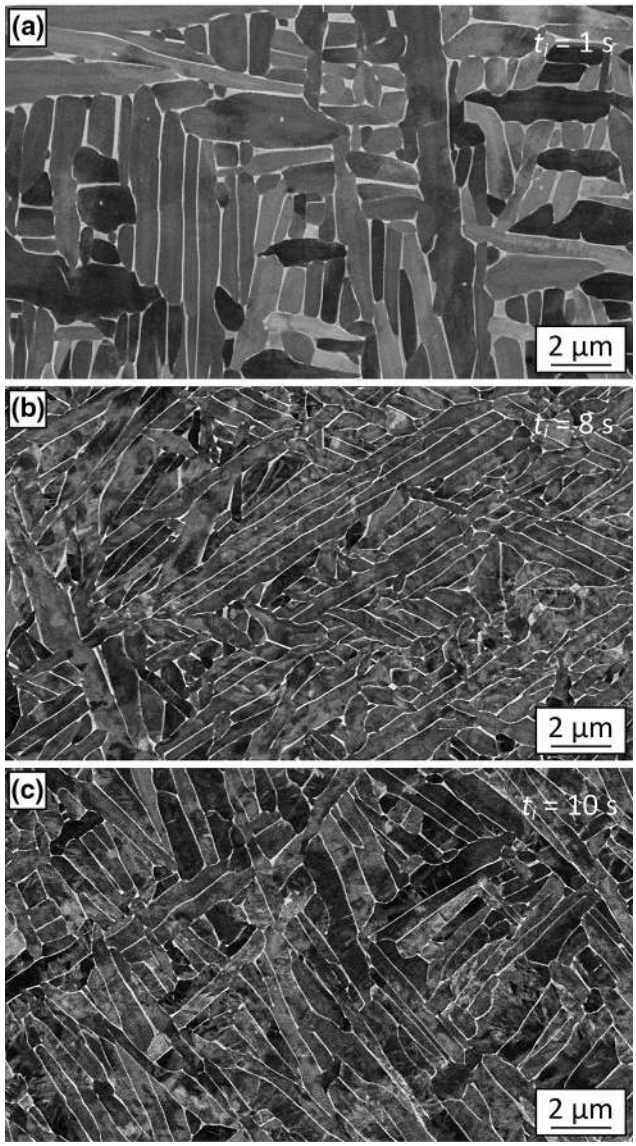

Fig. 1. Microstructures at the height of 15 mm in the SLM-fabricated 30-mm-tall samples with inter-layer times of (a) 1 s, (b) 8 s and (c) 10 s. The β phase has a bright contrast, and the α phase has a gray contrast.

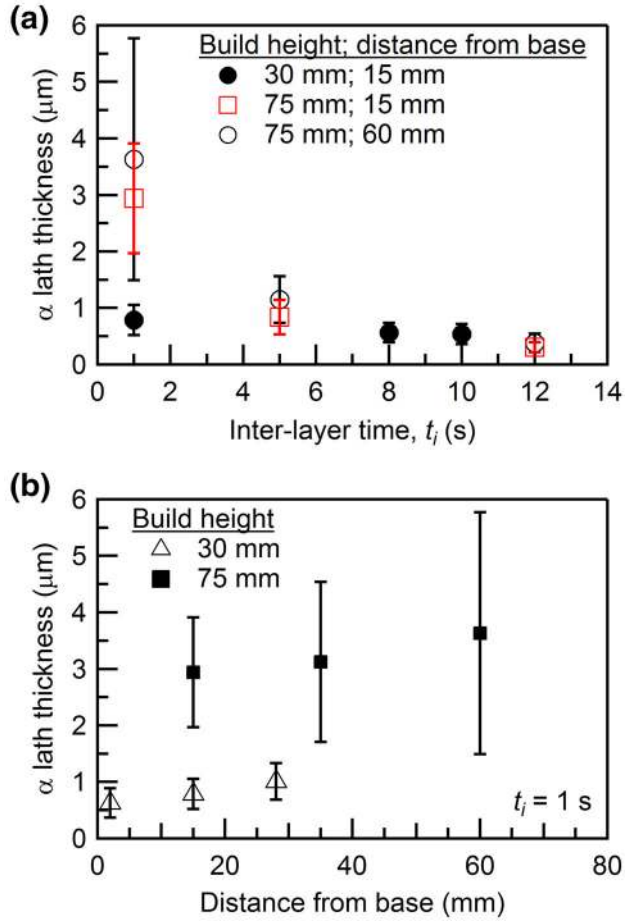

Fig. 2. Variation of the α-lath thickness in the SLM-fabricated 30-mm- and 75-mm-tall samples as a function of (a) inter-layer time at a specific height and (b) height along the build direction at inter-layer time of 1 s.

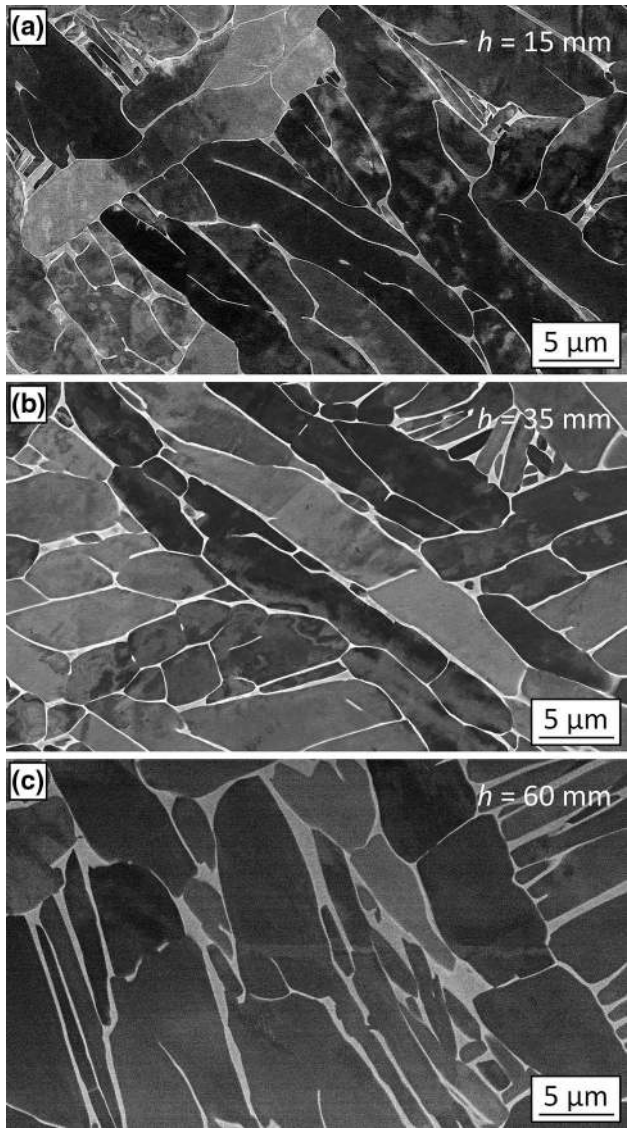

Fig. 3. Microstructure variation along the build direction in the SLM-fabricated 75-mm-tall sample with an inter-layer time of 1 s. (a) 15 mm, (b) 35 mm and (c) 60 mm. The β phase has a bright contrast, and the α phase has a gray contrast.

direction of the 75-mm-tall sample, the microstructures at the heights of 15 mm, 35 mm, and 60 mm with t_i = 1 s were examined (Fig. 3), and the α-lath thickness increased marginally from 2.94 μm ± 0.97 μm at 15 mm, to 3.12 ± 1.42 μm at 35 mm and then to 3.63 ± 2.14 μm at 60 mm (Fig. 3b). The α-laths at the bottom (Fig. 3a) were finer than those in the middle (Fig. 3b) and the upper sections (Fig. 3c). A similar trend was found in the 30-mm-tall sample (Fig. 2b, 0.63 ± 0.26 μm at 2 mm, 0.79 ± 0.26 μm at 15 mm, 1.01 ± 0.32 μm at 28 mm). Figure 2b indicates that the variation of microstructure along the build height is marginal in both the 30-mm- and 75-mm-tall samples. The key innovation we have demonstrated here is that SLM-fabricated Ti–6Al–4V can achieve a fully lamellar α + β microstructure in the as-built state at the layer thickness of 90 μm and this can enable much larger parts to be built with a wider processing window.

In Ti–6Al–4V, β → α′ martensitic transformation occurs when the cooling rate is greater than ~ 410 K/s,[13,14] and massive transformation takes place when reducing the cooling rate to the range of 20–410 K/s. Further decreasing the cooling rate to below 20 K/s leads to the formation of lamellar α plates in the prior β grains. During SLM, the cooling rate of the melt pool during solidification is typically in the range of 10^3–10^5 K/s.[2] The subsequent solid-state cooling process occurs at different cooling rates specific to build height for fixed SLM parameters. The presence of continuous grain boundary (GB) α and coarse α-laths at the height of 60 mm in the 75-mm-tall samples with t_i = 1 s (Fig. 4) are indicative of slow cooling rates and/or high temperature retention during a certain period of the solid-state cooling process as a result of the new processing parameters adopted in this study. As a result of a longer period of continuous subsequent heating, noticeable coarsening of the α-laths occurred at the

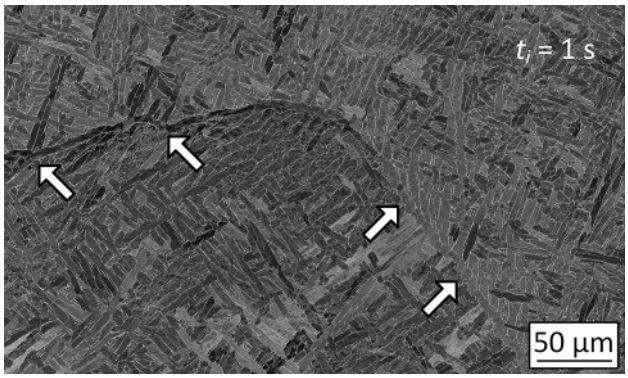

Fig. 4. Microstructure at the height of 60 mm in the SLM-fabricated 75-mm-tall sample with an inter-layer time of 1 s, showing coarse α-laths and continuous GB α (arrowed).

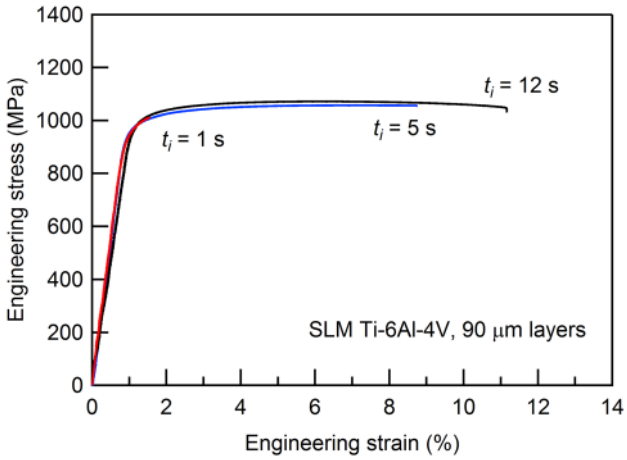

Fig. 5. Engineering tensile stress–strain curves of the SLM-fabricated Ti–6Al–4V samples produced using different inter-layer times.

same height in the 75-mm-tall samples as the 30-mm-tall samples (Fig. 2b). This also led to a greater extent of α-lath globularization.

Figure 5 shows the engineering tensile stress–strain curves for the 90-μm-layer samples made with inter-layer times of 1 s, 5 s, and 12 s. All three samples have similar yield stress of ~ 980 MPa. However, the sample built with t_i = 1 s fractured shortly upon yielding. In contrast, samples built with t_i = 12 s achieved tensile ductility of 11% in the as-built state. This distinct discrepancy, although unexpected, can be explained by the process-induced defects (porosity and lack of fusion) as shown on the fracture surface (Fig. 6). An analysis of the fracture surface revealed that the percentage of defects (area) and average defect size are respectively 16% and 59.4 μm for t_i = 1 s, 13.4% and 56.6 μm for t_i = 5 s, and 13.8% and 43.3 μm for t_i = 12 s. The pore size for t_i = 1 s is skewed heavily to larger sizes in which 24% of the pores are > 80 μm compared to 18% for t_i = 5 s and a7% for

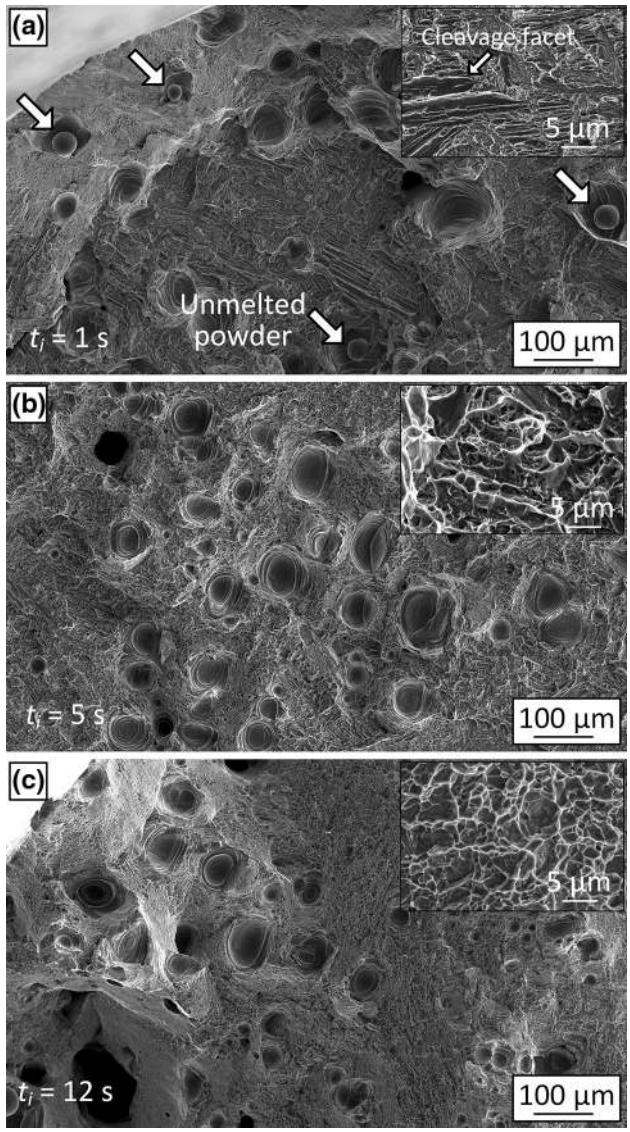

Fig. 6. Tensile fracture surfaces of SLM-fabricated Ti–6Al–4V samples with different inter-layer times of (a) 1 s, (b) 5 s and (c) 12 s. The insets are high-magnification SEM micrographs showing detailed features of the fracture surfaces.

t_i = 12 s. In addition, for the sample built with t_i = 1 s, a few un-melted powder particles were also observed within these pores (Fig. 6a, arrowed), while the fracture surfaces consisted of mostly quasi-cleavage facets (inset). This is possibly due to the presence of both lack of fusions and continuous GB α. With t_i = 5 s (Fig. 6b), the fracture surface showed a mixture of quasi-cleavage facets and ductile dimples, while with t_i = 12 s (Fig. 6c), ductile dimples were dominant with a limited presence of quasi-cleavage facets. The trend of quasi-cleavage facets increasing with decreasing t_i corresponds well with the decreasing trend in tensile ductility obtained from those samples.

It was found that defects were consistently more prevalent in the 75-mm-tall samples than in the 30-mm-tall samples. Although the exact reason is unclear, the slower cooling rate with increasing build height, as evident from the much coarser microstructure observed in the 75-mm-tall samples, may have played an influential role. It is likely that the melt pool stability has changed as a result of the changed temperature profiles. Further work is needed to clarify this in the future.

SUMMARY

- Fully lamellar $\alpha + \beta$ microstructures were produced in SLM-fabricated Ti–6Al–4V using a layer thickness of 90 μm. The build height and inter-layer time are both influential in determining the α-lath thickness and morphology. The influence of build height on α-lath thickness is more pronounced with the use of shorter inter-layer times.
- Tensile fractography showed a noticeable presence of process-induced defects in the 75-mm-tall samples, which, together with the presence of continuous GB α, resulted in low ductility for those with coarse lamellar structures (t_i of 1 s). Fine lamellar microstructures (t_i of 12 s) proved to be less sensitive to the presence of similar defects and achieved a good combination of tensile ductility (11%) and yield strength (980 MPa) in the as-built state.
- Both the microstructural and tensile property results obtained from this study are promising for broadening the processing window to achieve fully lamellar $\alpha + \beta$ microstructures for SLM of Ti–6Al–4V. Further work is needed to fine-tune the processing parameters with respect to different sample dimensions.

ACKNOWLEDGEMENTS

This project was funded by the Australian Research Council (ARC) through ARC DP150104719. WX appreciates financial support from the Macquarie University Research Development Grants (9201601532). The authors acknowledge the technical assistance of the RMIT Microscopy and Microanalysis Facility.

REFERENCES

1. L. Thijs, F. Verhaeghe, T. Craeghs, J.V. Humbeeck, and J.P. Kruth, *Acta Mater.* 58, 3303 (2010).
2. M. Qian, W. Xu, M. Brandt, and H.P. Tang, *MRS Bull.* 41, 775 (2016).
3. B. Vandenbroucke and J.P. Kruth, *Rapid Prototyping J.* 13, 196 (2007).
4. G. Lütjering, *Mat. Sci Eng. A.* 243, 32 (1998).
5. J.J. Lewandowski and M. Seifi, *Ann Rev Mater Res.* 46, 151 (2016).
6. T. Vilaro, C. Colin, and J.D. Bartout, *Metall. Mater. Trans. A* 42, 3190 (2011).
7. W. Xu, S. Sun, J. Elambasseril, Q. Liu, M. Brandt, and M. Qian, *JOM* 67, 668 (2015).
8. W. Xu, E.W. Lui, A. Pateras, M. Qian, and M. Brandt, *Acta Mater.* 125, 390 (2017).
9. P. Barriobero-Vila, J. Gussone, J. Haubrich, S. Sandlöbes, J. Da Silva, P. Cloetens, N. Schell, and G. Requena, *Materials* 10, 268 (2017).
10. W. Xu, M. Brandt, S. Sun, J. Elambasseril, Q. Liu, K. Latham, K. Xia, and M. Qian, *Acta Mater.* 85, 74 (2015).
11. M. Ma, Z. Wang, M. Gao, and X. Zeng, *J. Mater. Process. Tech.* 215, 142 (2015).
12. S. Bremen, W. Meiners, and A. Diatlov, *Laser Tech. J.* 9, 33 (2012).
13. J. Sieniawski, W. Ziaja, K. Kubiak, and M. Motyka, in *Titanium Alloys—Advances in Properties Control*, ed. J. Sieniawski and W. Ziaja (InTech, Rijeka, 2013), p. 69.
14. T. Ahmed and H.J. Rack, *Mater. Sci. Eng. A* 243, 206 (1998).